

## Multiple Auger decay of the neon 1s-core-hole state studied by multielectron coincidence spectroscopy

Y. Hikosaka,<sup>1</sup> T. Kaneyasu,<sup>2</sup> P. Lablanquie,<sup>3,4</sup> F. Penent,<sup>3,4</sup> E. Shigemasa,<sup>5</sup> and K. Ito<sup>6</sup>

<sup>1</sup>*Graduate School of Medicine and Pharmaceutical Sciences, University of Toyama, Toyama 930-0194, Japan*

<sup>2</sup>*SAGA Light Source, Tosu 841-0005, Japan*

<sup>3</sup>*Sorbonne Universités, UPMC, Université Paris 06, Laboratoire de Chimie Physique-Matière et Rayonnement, 11 rue Pierre et Marie Curie, 75231 Paris Cedex 05, France*

<sup>4</sup>*CNRS, LCPMR (UMR 7614), 11 rue Pierre et Marie Curie, 75231 Paris Cedex 05, France*

<sup>5</sup>*UVSOR Facility, Institute for Molecular Science, Okazaki 444-8585, Japan*

<sup>6</sup>*Photon Factory, Institute of Materials Structure Science, Tsukuba 305-0801, Japan*

(Received 20 April 2015; published 14 September 2015)

The Auger decay processes from the 1s-core-hole state of Ne have been investigated with a multielectron coincidence method. We have observed the double and triple Auger decays, in which both cascade and direct processes are identified from different ways in energy sharing between the Auger electrons. Branching ratios for the different electronic configurations of the Auger final states are determined from the corresponding electron coincidence yields. Particularly for the double Auger decay, the branching ratios are divided into the individual contributions from direct and cascade paths.

DOI: [10.1103/PhysRevA.92.033413](https://doi.org/10.1103/PhysRevA.92.033413)

PACS number(s): 32.80.Fb, 32.80.Hd

### I. INTRODUCTION

Auger decay is the predominant pathway in the relaxations of the inner-shell vacancies in light elements. Nowadays it is known that, apart from the usual Auger decay with the emission of one electron, processes in which two or more Auger electrons are emitted constitute sizable fractions in the total Auger intensity. The first experimental evidence for emissions of two Auger electrons (double Auger decay) was brought forward by detecting Ne<sup>3+</sup> ions formed in the Ne 1s decay [1,2]. Later experiments on the double Auger (DA) decay, which are also based on photoion detection, determined more accurately the fraction of the contribution (~6%) in the total Ne 1s decay [3,4].

Many theoretical efforts have been made to interpret the probability of the DA decay in Ne. The calculations with consideration of only monopole process (shakeoff) yield apparently smaller values (0.5% [2] or 0.7% [5]). Improvement has been achieved by taking account of electron correlation [4,6,7]. Particularly the calculation considering the final-state correlations of core electrons and correlations of core electrons with Auger electrons results in the DA probability of 5.39%, which is the best agreement with the experiment [7].

The emission of the two electrons in DA decay can be simultaneously or in a stepwise manner through the creation and the decay of an intermediate Ne<sup>2+</sup> state. The former and latter processes are denoted by direct DA decay and cascade DA decay, respectively. While the theoretical calculations deal basically with direct DA decay, the experimental Ne<sup>3+</sup> intensity includes the contribution from cascade DA decay. On that account, the comparison between the experimental Ne<sup>3+</sup> intensity and the calculations may not be a valid test of the theoretical frameworks.

The contributions from direct and cascade DA decays can be identified by electron coincidence measurements, because these DA paths show different ways in energy sharing between the two Auger electrons. Vieffhaus *et al.* observed the energy distribution of the electrons emitted by the DA decay processes in Ne, by means of electron coincidence spectroscopy [8].

While a continuous energy sharing corresponding to the direct DA decay was clearly presented, the energy resolution was insufficient to resolve the Ne<sup>3+</sup> states produced by the DA decay and discrete peaks due to the cascade DA decay.

In the present study, we have performed, by using a magnetic bottle electron spectrometer, a multielectron coincidence study of the Ne 1s Auger decay, and obtained comprehensive information of the Auger decay. The powerful capability of the spectrometer in multielectron coincidence observations has been proved in its applications to the Auger decay processes in other rare gases [9–14]. In the electron coincidence data obtained, we have isolated the DA processes and clarified the contributions from direct and cascade paths. The branching ratios determined for the direct path for the formation of Ne<sup>3+</sup> are subject to a comparison with available calculations. In addition, the triple Auger (TA) decay is identified and the branching ratios of the final Ne<sup>4+</sup> states are obtained.

### II. EXPERIMENT

The experiments were performed at the undulator beamline BL-16A of the Photon Factory, during the single bunch operation of the storage ring that provides light pulses of 624 ns period. Synchrotron radiation was monochromatized by a grazing incidence monochromator using a varied-line-spacing plane grating. A mechanical chopper based on modification of a turbomolecular pump [15] was employed to block a certain fraction of the light pulses, thereby stretching the light pulse period to 12.5  $\mu$ s. Multielectron coincidence spectroscopy was performed by using a magnetic bottle electron spectrometer [16]. The description of the spectrometer and the data accumulation scheme is given elsewhere [15]. Conversion of the electron time of flight to kinetic energy was achieved by measuring the Ar photoelectron spectral lines at different photon energies. It was estimated that the energy resolving power of the apparatus,  $E/\Delta E$ , was nearly constant at 60 for electrons of  $E > 3$  eV, though  $\Delta E$  was limited to around 20 meV (FWHM) for  $E < 1$  eV. The measured detection

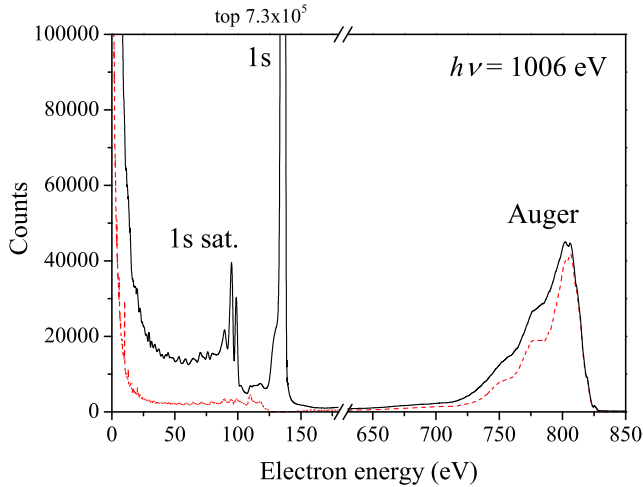


FIG. 1. (Color online) Histogram (black solid) of the energies of all the electrons, derived from the coincidence data set accumulated at a photon energy of 1006 eV for Ne, and the Auger yields (red broken) observed in coincidences with the 1s photoelectrons. The intensity of the coincidence Auger spectrum was multiplied by a factor of 1.5, in order to compensate the detection efficiency ( $\sim 65\%$ ) of the photoelectrons.

efficiency decreases slowly with electron kinetic energy from  $75 \pm 5\%$  ( $E \approx 0$  eV) to  $40 \pm 5\%$  ( $E \approx 800$  eV).

### III. RESULTS AND DISCUSSION

#### A. Total electron spectrum and coincidence Auger spectrum

A multielectron coincidence data set was accumulated at a photon energy of 1006 eV for Ne, with a count rate around 3 kHz during an accumulation time of 12 h. The photon bandwidth was set to around 2 eV. This photon energy,  $\sim 136$  eV above the Ne 1s binding energy (870.09 eV [17]), was chosen in order to avoid an overlap between the photoelectron and the important Auger structures.

An electron energy spectrum derived from the total events in the coincidence data set is shown in Fig. 1. The 1s photoelectron peak is exhibited at a kinetic energy of  $\sim 136$  eV, and the satellite structures corresponding to the formation of the  $1s^{-1}2l^{-1}nl'$  states [18] lie in the kinetic energy range of 80–100 eV. On the lower kinetic energy side of the satellite structures, a continuous distribution increasing in intensity with decreasing kinetic energy is observed. A substantial fraction of the electron yields is due to core-valence double photoionization forming  $1s^{-1}2l^{-1}$  states [19], which produces two photoelectrons sharing the available energy and thus having a continuous energy distribution.

The Auger structure observed in 700–850 eV contains the contributions from the single Auger decays of the  $1s^{-1}$ , satellite  $1s^{-1}2l^{-1}nl'$ , and core-valence  $1s^{-1}2l^{-1}$  states. The individual contributions can be extracted by analyzing energies of electrons in coincidence, and the Auger spectra associated with the decays of the satellite and core-valence states were already reported [19,20]. In Fig. 1, the Auger yields observed in coincidences with the 1s photoelectrons are plotted (red broken line). Here, the intensity of the coincidence Auger spectrum was multiplied by a factor of 1.5, in order to compensate the detection efficiency ( $\sim 65\%$ ) of the photoelectrons. Beside

TABLE I. Partial probabilities of double Auger decay in the total decay of Ne 1s. The values are in percent.

Final $\text{Ne}^{3+}$ state	Total DA	Cascade		Direct		
		path	path	Calc <sup>a</sup>	Calc <sup>b</sup>	Calc <sup>c</sup>
$2p^{-3}$	2.5	1.6	0.9	2.54	1.64	} 2.5
$2s^{-1}2p^{-2}$	2.9	1.2	1.7	2.14	1.18	
$2s^{-2}2p^{-1}$	0.5		0.5	0.71	0.19	
Sum	5.97 <sup>b</sup>	2.8	3.2	5.39	3.1	4

<sup>a</sup>Reference [7].

<sup>b</sup>Reference [4].

<sup>c</sup>Reference [6].

the structures in 700–850 eV due to the single Auger decay, the coincidence Auger spectrum exhibits continuous electron yields which remarkably increase down to zero kinetic energy. The electron yields are due to the DA and TA processes of the  $1s^{-1}$  state, as clarified in the following subsections.

#### B. Double Auger decay

The DA decay of the  $1s^{-1}$  state can be observed as triple coincidences of a 1s photoelectron and two Auger electrons. The population of the  $\text{Ne}^{3+}$  states formed by the DA decay is revealed by plotting the coincidence yields as a function of the sum of the energies of the two Auger electrons. The resultant spectrum is shown in Fig. 2(a), where the axis of the binding energy of the  $\text{Ne}^{3+}$  final states, converted with the relation of ( $\text{Ne}^{3+}$  binding energy) = ( $\text{Ne}^+ 1s^{-1}$  binding energy) – (the sum of the energies of the two Auger electrons), is also attached. The locations of the individual  $\text{Ne}^{3+}$  levels [21] are indicated with vertical bars. The limited energy resolution prevents us from identifying individual  $\text{Ne}^{3+}$  Auger final states, and three band structures attributed to  $\text{Ne}^{3+}$  states with the configurations of  $2p^{-3}$ ,  $2s^{-1}2p^{-2}$ , and  $2s^{-2}2p^{-1}$  are observed. By a peak fit assuming Gaussian peak shape, the relative populations of these configurations are determined to be  $(2p^{-3}) : (2s^{-1}2p^{-2}) : (2s^{-2}2p^{-1}) = 5.0 : 5.8 : 1$  [see Fig. 2(a)]. From the relative populations determined and the total DA probability reported (5.97% [4]), the probabilities of the DA processes forming the individual configurations of  $\text{Ne}^{3+}$ , presented in Table I, are estimated.

The probabilities derived for the DA processes are constituted of the contributions from the direct and cascade paths. These two contributions show different ways in energy sharing between the two Auger electrons emitted. Figure 3 displays an energy correlation map for the two Auger electrons included in the triple coincidences, revealing the energy sharing between the Auger electrons. Three diagonal stripes corresponding to the  $\text{Ne}^{3+}$  structures in Fig. 2(a) are observed on the map. Note that the integration of the counts on the map along the direction for (fast Auger electron energy) + (slow Auger electron energy) = const. essentially corresponds to the spectrum in Fig. 2(a).

The two Auger electrons emitted in the direct path of the DA decay share continuously the available energy given by ( $\text{Ne}^+ 1s^{-1}$  binding energy) – ( $\text{Ne}^{3+}$  binding energy). Thus the continuous intensities along the three diagonal stripes seen in Fig. 3 are due to the direct path for the formation of the  $\text{Ne}^{3+}$  final states. On the diagonal stripes, intense island

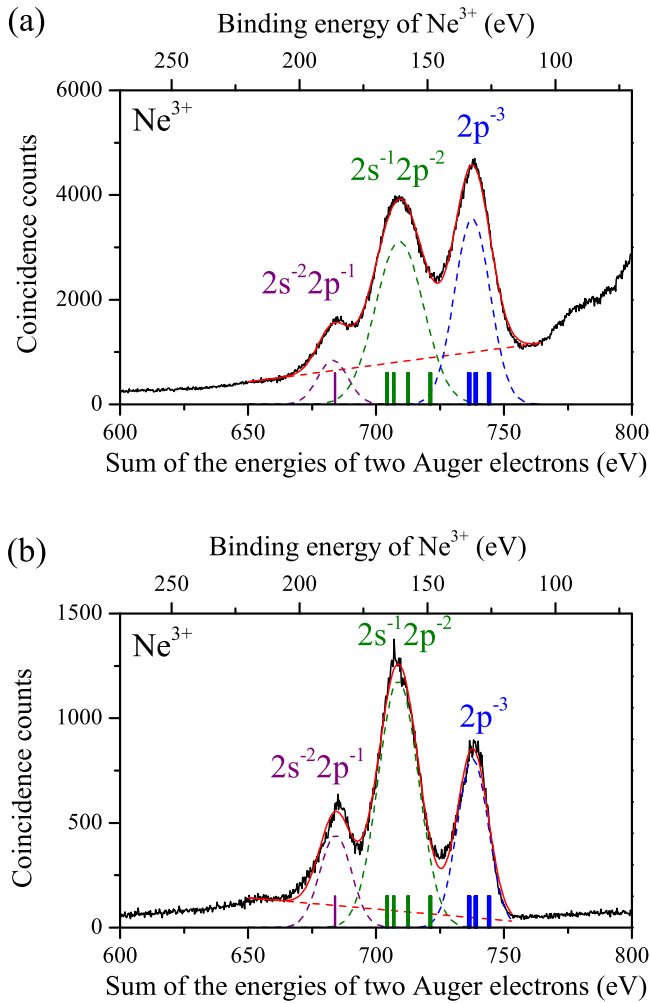


FIG. 2. (Color online) Histograms (black solid) of the energy sums of two Auger electrons detected in coincidence with 1s photoelectrons, obtained (a) for the Auger electrons in the whole energy range and (b) for the Auger electrons in the magnified area in Fig. 3. The observed structures are due to the  $\text{Ne}^{3+}$  states produced by the DA decay of the  $1s^{-1}$  state. The binding energies of the individual levels of  $\text{Ne}^{3+}$  [21] are indicated with vertical bars, where the states with the configurations of  $2p^{-3}$ ,  $2s^{-1}2p^{-2}$ , and  $2s^{-2}2p^{-1}$  are shown in blue, green, and purple, respectively. Red solid curves are the fitting results assuming three Gaussian peaks, and the individual contributions are drawn with broken lines. Note that intensity outside the three Gaussian peaks, especially in the range of 750–800 eV in (a), basically come from false coincidences.

structures are exhibited in the slow Auger electron's energy range of 0–30 eV (bottom right area in this map). These structures result from the cascade DA path. The coordinates of the island structures are defined by the discrete kinetic energies of the two Auger electrons; the fast Auger electrons depict the  $\text{Ne}^{2+}$  states populated above the  $\text{Ne}^{3+}$  threshold, and the energies of the slow Auger electrons correspond to the energy differences between these  $\text{Ne}^{2+}$  states and final  $\text{Ne}^{3+}$  states.

To locate the Auger lines of the second step in the cascade path, the intensities along the three diagonal lines on the energy correlation map are shown in Fig. 4. Peaks due to the cascade

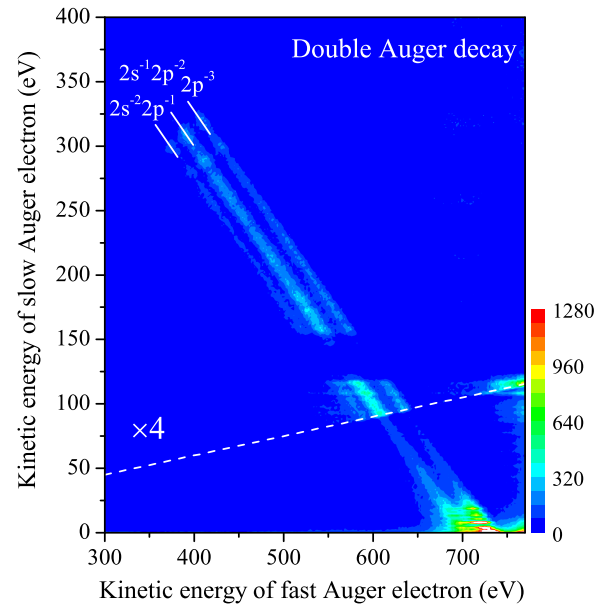


FIG. 3. (Color online) Energy correlation map for the two Auger electrons detected in coincidence with 1s photoelectrons. The intensity in the area of  $y > x \times 0.15$  is magnified by a factor of 4, in order to improve the visibility of weak structures. A blind area arises in the slow Auger electron's energy range of 120–150 eV, because the signals of Auger electrons in the corresponding time-of-flight range are undetected due to the overlap with photoelectron signals.

DA path are extensively observed in the formations of the  $2p^{-3}$  and  $2s^{-1}2p^{-2}$  states. In contrast, the contribution from the cascade path is negligibly small in the formation of  $2s^{-2}2p^{-1}$ . Unfortunately, information of the  $\text{Ne}^{2+}$  states lying above the  $\text{Ne}^{3+}$  threshold is very limited [20,21], and we cannot give any tangible assignments to the observed peaks. It should be noted that the same  $\text{Ne}^{2+}$  states as involved in the cascade DA processes from the Ne 1s satellites with the configuration of  $1s^{-1}2p^{-1}3p$  [20] are hardly identified in Fig. 4. The intermediate  $\text{Ne}^{2+}$  states populated in the DA decay of the satellite states are mostly excited in low- $n$  Rydberg states, due to the preferred spectator behavior of the  $3p$ -excited electron in the initial states. It is manifested that such Rydberg-excited  $\text{Ne}^{2+}$  states are rarely populated in the cascade DA decay of  $\text{Ne}^+ 1s^{-1}$ .

The distribution for the formation of  $2s^{-2}2p^{-1}$  (the top panel in Fig. 4), which is essentially free from cascade DA contribution, presents a part of a so-called U-shape profile, in qualitative agreement with a calculation result [6]. The distribution is well reproduced by a sum of two exponential decay curves, as shown with the red broken curve in this figure. Fairly similar profiles are observed in the continuous distributions due to direct DA paths for the formations of  $2p^{-3}$  and  $2s^{-1}2p^{-2}$ . In practice, these continuous distributions can be reproduced with the fit curve for the  $2s^{-2}2p^{-1}$  channel (red broken curves), by multiplying proper factors.

Figure 2(b) shows the histogram of the kinetic energy sum of the two Auger electrons, which is obtained for the magnified area in Fig. 3 and thus by masking the contribution of cascade DA decay. The relative intensities of the three band structures are determined to be  $(2p^{-3}) : (2s^{-1}2p^{-2}) : (2s^{-2}2p^{-1}) = 1.8 :$

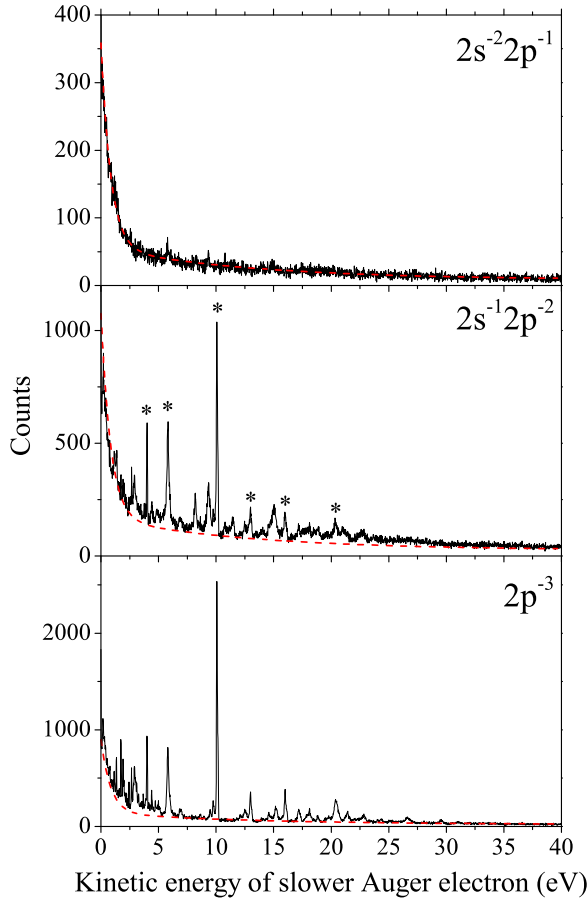


FIG. 4. (Color online) Energy distributions of slow electrons emitted in the DA decay of the  $1s^{-1}$  state into the  $2p^{-3}$ ,  $2s^{-1}2p^{-2}$ , and  $2s^{-2}2p^{-1}$  of  $\text{Ne}^{3+}$ . The ranges of the sum of the energies of two Auger electrons, set in the extraction of these distributions, are 670–690 eV, 690–725 eV, and 725–755 eV. Peaks indicated by asterisks in the  $2s^{-1}2p^{-2}$  channel are contaminations from the  $2p^{-3}$  channel. The red broken curve in the top panel shows a fit result to the  $2s^{-2}2p^{-1}$  curve by using a function of a sum of two exponential decay curves, and the curves obtained by multiplying proper factors to the fit result are plotted in the middle and bottom panels.

3.4 : 1, by a peak fit assuming Gaussian peak shape. It can be regarded that, because similar profiles are observed in the energy distributions of the direct DA paths for these channels, the relative intensities determined in Fig. 2(b) correspond to the branching ratio of the direct DA contributions. Considering that the cascade DA contribution is negligible in the  $2s^{-2}2p^{-1}$  channel, the decreases of the relative intensities of the other two channels are attributable to the cascade DA contributions. The probabilities of the direct and cascade DA processes for these three channels thus estimated are summarized in Table I.

The cascade DA contributions share large fractions (64% and 38%) in the total DA intensities of the  $2p^{-3}$  and  $2s^{-1}2p^{-2}$  channels, and thus the ratio of the direct DA paths differs much from that of the total DA processes. The ratio of the direct DA paths accords roughly with the statistical weights of the final states,  $(2p^{-3}) : (2s^{-1}2p^{-2}) : (2s^{-2}2p^{-1}) = 20 : 30 : 6$ . Although available calculations [4,7] provide the probabilities

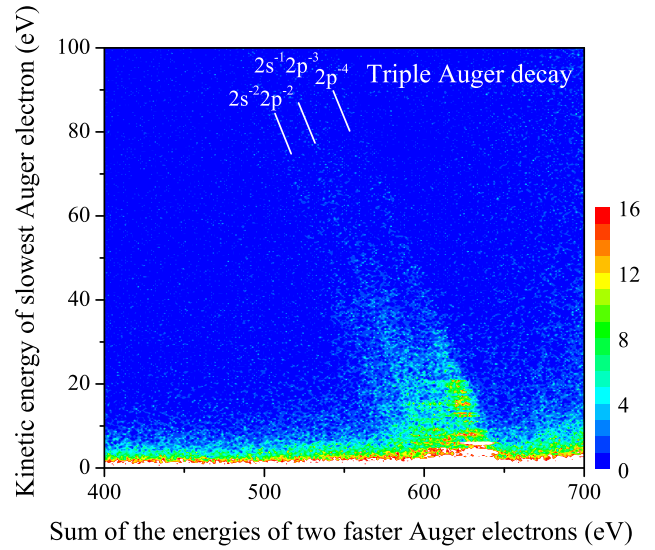


FIG. 5. (Color online) Energy correlation map displaying the three Auger electrons in coincidence with  $1s$  photoelectrons, where the coincidence yields are plotted as a function of the sums of the faster two Auger electrons and of kinetic energy of the slowest Auger electron.

for the formations of final states consisting of  $\text{Ne}^{3+}$  core and one excited or ejected electron, it is expected that the calculated probabilities can be compared with the experimental direct DA probabilities. However, the available calculations do not agree even qualitatively with the experimental probabilities of the direct DA path. In particular, we can find that the calculations in Refs. [4,7] possibly overestimate the  $2p^{-3}$  channel, compared to the other channels.

### C. Triple Auger decay

The TA decay of the  $1s^{-1}$  state can be observed as quadruple coincidences of a  $1s$  photoelectron and three Auger electrons. The two-dimensional map in Fig. 5 displays the energy correlations among the three Auger electrons in the quadruple coincidences including  $1s$  photoelectron. Here, the coincidence yields are plotted as a function of the sum of the kinetic energies of the two faster Auger electrons (horizontal axis), and of kinetic energy of the slowest Auger electron (vertical axis). In this plot, the coincidences between the three Auger electrons emitted for the formation of a particular  $\text{Ne}^{4+}$  state lie on a diagonal line defined by (sum of the kinetic energies of the faster two Auger electrons) + (slowest Auger electron energy) =  $(\text{Ne}^+ 1s^{-1} \text{ binding energy}) - (\text{Ne}^{4+} \text{ binding energy})$ . In practice, several diagonal stripes for formation of  $\text{Ne}^{4+}$  levels are identified on this map. One can find island structures on the diagonal stripes.

Figure 6 shows the coincidence yields as a function of the sum of the energies of the three Auger electrons, corresponding to the integration of the coincidence counts in Fig. 5 along the direction for (sum of the kinetic energies of the faster two Auger electrons) + (slowest Auger electron energy) = const. The spectrum reveals the population of the  $\text{Ne}^{4+}$  states formed by the TA decay. A fit using four Gaussian peaks reproduces

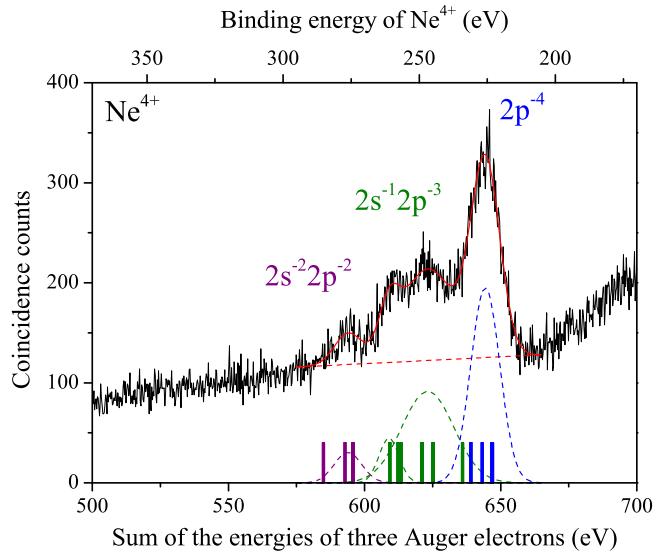


FIG. 6. (Color online) Histogram of the kinetic energy sum of the three Auger electrons observed in coincidence with  $1s$  photoelectrons. The energy levels for the individual  $\text{Ne}^{4+}$  states [21] are indicated, where the states with the configurations of  $2p^{-4}$ ,  $2s^{-1}2p^{-3}$ , and  $2s^{-2}2p^{-2}$  are shown in blue, green, and purple, respectively. Red solid curves are the fitting results assuming four Gaussian peaks, and the individual contributions are drawn with broken lines.

well the observed  $\text{Ne}^{4+}$  structures. Compared to the literature values of the individual  $\text{Ne}^{4+}$  levels [21] indicated with vertical bars, these band structures are assigned to  $2p^{-4}$ ,  $2s^{-1}2p^{-3}$  and  $2s^{-2}2p^{-2}$ , where both the middle two bands are allocated to  $2s^{-1}2p^{-3}$ . The relative intensities are determined to be  $(2p^{-4}) : (2s^{-1}2p^{-3}) : (2s^{-2}2p^{-2}) = 6.8 : 6.7 : 1$ . Because the total TA probability is reported to be 0.38% [4], the probabilities of the TA processes forming the configurations of  $2p^{-4}$ ,  $2s^{-1}2p^{-3}$ , and  $2s^{-2}2p^{-2}$  of  $\text{Ne}^{4+}$  are estimated as 0.18%, 0.18%, and 0.03%, respectively.

The intensity distributions along the diagonal lines in Fig. 5 for the formation of  $2p^{-4}$ ,  $2s^{-1}2p^{-3}$ , and  $2s^{-2}2p^{-2}$ , delineating the energies of the slowest Auger electrons emitted in the TA processes, are presented in Fig. 7. Intense peaks are observed in the  $2p^{-4}$  and  $2s^{-1}2p^{-3}$  channels, while such peaks are not remarkable in the  $2s^{-2}2p^{-2}$  channel. The electron emissions of these discrete energies are due to cascade TA processes. Here, two categories can be considered: (1) fully sequential three electron emissions,  $1s^{-1} \rightarrow (2s2p)^{-2} + e^{-} \rightarrow (2s2p)^{-3} + 2e^{-} \rightarrow (2s2p)^{-4} + 3e^{-}$ , and (2) direct DA followed by subsequent single Auger electron emission,  $1s^{-1} \rightarrow (2s2p)^{-3} + 2e^{-} \rightarrow (2s2p)^{-4} + 3e^{-}$ . While the former process emits three Auger electrons with discrete energies, in the latter process two electrons emitted in the first step show distributed energies.

Figure 8 shows the energy correlation between the slower two Auger electrons emitted in all TA decays. Although statistics is poor, one finds on the map horizontal lines which are constructed by coincidences between electrons of discrete and distributing energies. In contrast, spot structures due to two electrons of discrete energies are scarcely discernible. These observations suggest that the formation of intermediate

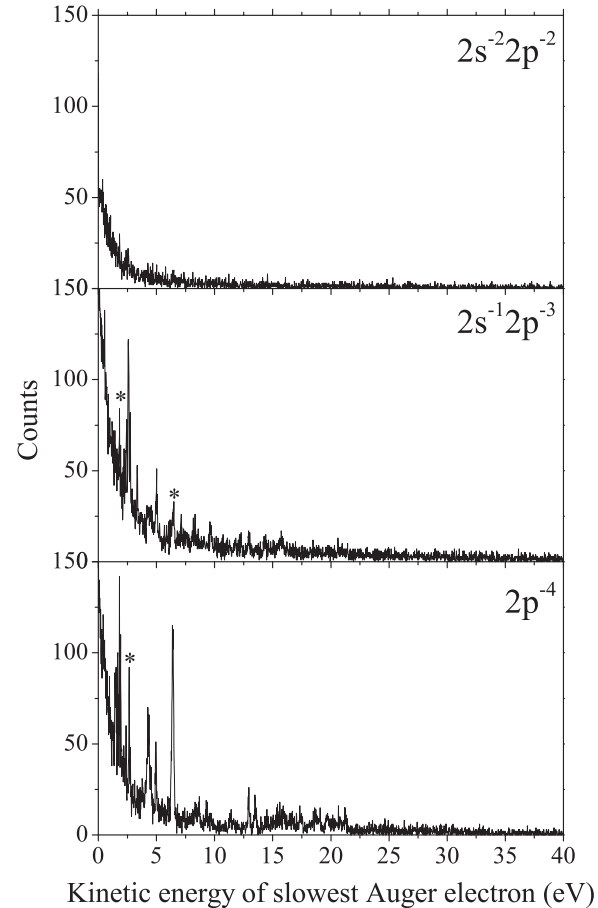


FIG. 7. Energy distributions of the slowest electrons emitted in the TA decay of the  $1s^{-1}$  state into the  $2p^{-4}$ ,  $2s^{-1}2p^{-3}$ , and  $2s^{-2}2p^{-2}$  of  $\text{Ne}^{4+}$ . The ranges of the sum of the energies of the three Auger electrons, set in the extraction of these distributions, are 588–601 eV, 601–632 eV, and 632–656 eV. Peaks indicated by asterisks in the  $2p^{-4}$  and  $2s^{-1}2p^{-3}$  channel are contaminations from each other.

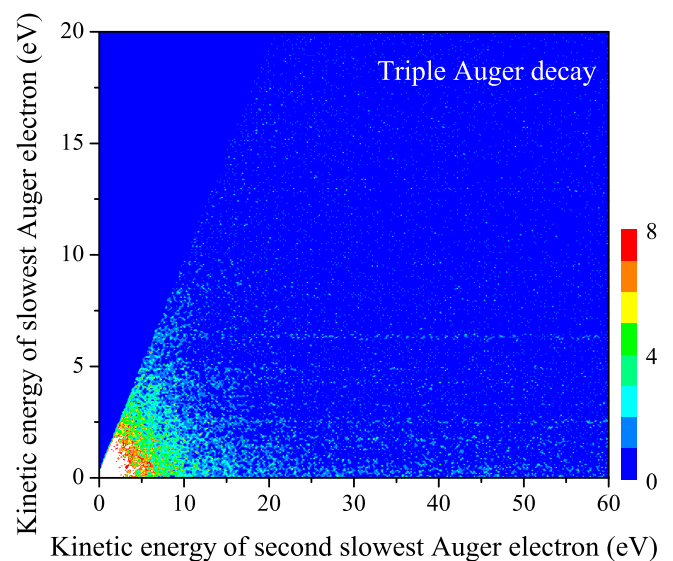


FIG. 8. (Color online) Two-dimensional map of energy correlation between slower two Auger electrons emitted in the TA decay of the  $1s^{-1}$  state.

Ne<sup>3+</sup> states by direct DA decay and the subsequent single electron emissions constitute the dominant path of the cascade TA decay.

#### IV. CONCLUSIONS

The multiple Auger decay of the  $1s^{-1}$  state in Ne has been investigated with a multielectron coincidence method. The energy correlation information enables us to identify cascade and direct processes in both the DA and TA decays. Branching ratios are determined to the different electronic configurations

of the final Ne<sup>3+</sup> (Ne<sup>4+</sup>) states populated by the DA (TA) decay. Moreover, for the DA decay, we have clarified the contributions from direct and cascade paths.

#### ACKNOWLEDGMENTS

We are grateful to the Photon Factory staff for the stable operation of the PF ring. Financial support from JSPS and CNRS are acknowledged. This work was performed with the approval of the Photon Factory Program Advisory Committee (Proposals No. 2006G230 and No. 2008G519).

- 
- [1] M. O. Krause, M. L. Vestal, W. H. Johnston, and T. A. Carlson, *Phys. Rev.* **133**, A385 (1964).
- [2] T. A. Carlson and M. O. Krause, *Phys. Rev. Lett.* **14**, 390 (1965).
- [3] N. Saito and I. H. Suzuki, *Phys. Scr.* **49**, 80 (2000).
- [4] B. Kanngießer, M. Jainz, S. Brünken, W. Bente, Ch. Gerth, K. Godehusen, K. Tiedtke, P. van Kampen, A. Tutay, P. Zimmermann, V. F. Demekhin, and A. G. Kochur, *Phys. Rev. A* **62**, 014702 (2000).
- [5] A. G. Kochur, V. L. Sukhorukov, A. J. Dudenko, and Ph. V. Demekhin, *J. Phys. B* **28**, 387 (1995).
- [6] M. Ya. Amusia, I. S. Lee, and V. A. Kilin, *Phys. Rev. A* **45**, 4576 (1992).
- [7] A. G. Kochur, V. L. Sukhorukov, and Ph. V. Demekhin, *J. Electron Spectrosc. Relat. Phenom.* **137**, 325 (2004).
- [8] J. Viefhaus, A. N. Grum-Grzhimailo, N. M. Kabachnik, and U. Becker, *J. Electron Spectrosc. Relat. Phenom.* **141**, 121 (2004).
- [9] F. Penent, J. Palaudoux, P. Lablanquie, L. Andric, R. Feifel, and J. H. D. Eland, *Phys. Rev. Lett.* **95**, 083002 (2005).
- [10] Y. Hikosaka, P. Lablanquie, F. Penent, T. Kaneyasu, E. Shigemasa, J. H. D. Eland, T. Aoto, and K. Ito, *Phys. Rev. A* **76**, 032708 (2007).
- [11] P. Lablanquie, L. Andric, J. Palaudoux, U. Becker, M. Braune, J. Viefhaus, J. H. D. Eland, and F. Penent, *J. Electron Spectrosc. Relat. Phenom.* **156**, 51 (2007).
- [12] J. Palaudoux, P. Lablanquie, L. Andric, K. Ito, E. Shigemasa, J. H. D. Eland, V. Jonauskas, S. Kučas, R. Karazija, and F. Penent, *Phys. Rev. A* **82**, 043419 (2010).
- [13] E. Andersson, S. Fritzsche, P. Linusson, L. Hedin, J. H. D. Eland, J.-E. Rubensson, L. Karlsson, and R. Feifel, *Phys. Rev. A* **82**, 043418 (2010).
- [14] I. H. Suzuki, Y. Hikosaka, E. Shigemasa, P. Lablanquie, F. Penent, K. Soejima, M. Nakano, N. Kouchi, and K. Ito, *J. Phys. B* **44**, 075003 (2011).
- [15] K. Ito, F. Penent, Y. Hikosaka, E. Shigemasa, I. H. Suzuki, J. H. D. Eland, and P. Lablanquie, *Rev. Sci. Instrum.* **80**, 123101 (2009).
- [16] J. H. D. Eland, O. Vieuxmaire, T. Kinugawa, P. Lablanquie, R. I. Hall, and F. Penent, *Phys. Rev. Lett.* **90**, 053003 (2003).
- [17] A. P. Hitchcock and C. E. Brion, *J. Phys. B* **13**, 3269 (1980).
- [18] N. Mårtensson, S. Svensson, and U. Gelius, *J. Phys. B* **20**, 6243 (1987).
- [19] Y. Hikosaka, T. Aoto, P. Lablanquie, F. Penent, E. Shigemasa, and K. Ito, *Phys. Rev. Lett.* **97**, 053003 (2006).
- [20] Y. Hikosaka, T. Aoto, P. Lablanquie, F. Penent, E. Shigemasa, and K. Ito, *J. Phys. B* **39**, 3457 (2006).
- [21] NIST Atomic Spectra Database (version 3.1.5), available at <http://physics.nist.gov/asd3>.